PROGRESS IN LOW-COST ELECTRODEPOSITION OF $Cu(In,Ga)(S,Se)_2$: THE CISEL PROJECT

J. Kessler[1,2], J. Sicx-Kurdi[1], N. Naghavi[1], J.-F. Guillemoles[1], D. Lincot[1], O. Kerrec[1], M. Lamirand[3], L. Legras[3], P. Mogensen[4]

[1]Institut de Recherche et de Développement sur l'Energie Photovoltaïque (IRDEP, UMR 7174 CNRS-EDF-ENSCP)
6 quai Watier, 78401 Chatou, France
phone: +33 01 30 87 78 26, fax: +33 01 30 85 65, e-mail: john.kessler@univ-nantes.fr
[2]LAMP, Université de Nantes, 2 rue de la Houssinière, 44322 Nantes, France
[3]EDF R&D, Av des Renardières, Ecuelles, 77818 Moret-sur-Loing, France
[4]St. Gobain Recherche, 39 quai Lucien Lefranc, 93303 Aubervilliers, France

ABSTRACT: We pursue our development of the electrodeposition of $Cu(In,Ga)(S,Se)_2$ layers in view of a very low cost thin-film solar cell approach. The objective of the present contribution is to overview our full process flow chart and to examine in some detail specific material issues related to our approach. Chemical and structural aspects are examined by microscopy (scanning and transmission electron microscopy : SEM, TEM), as well as energy dispersive X-ray spectroscopy (EDX) and X-ray fluorescence (XRF) methods. In particular we here examine the recrystallization and sulfurization of Cu-rich precursors using x-rap diffraction (XRD). Some results from a typical array of devices, produced from 30x30 cm^2 precursor plates are shown.

Keywords: $CuInS_2$, Electrodeposition, Recrystallization

1 INTRODUCTION

In order for $Cu(In,Ga)(Se,S)_2$ (or CIGSS) based thin-film solar modules to become a market reality, low-cost production techniques are necessary, the goal must be production costs well below 1 €/W. The CISEL project is based on the application of electrodeposition as a low-cost process for the synthesis of the CIGSS absorber layer. The feasibility of this approach is a matter of increasing attention as reviewed in [1], and is the basis of the CISEL project [2]. Since the beginning of 2005 the IRDEP, *Institut de Recherche & Developpement sur l'Energie Photovoltaïque* (or Institute for Research and Development for Energy from Photovoltaics) has been founded as a UMR, *Unité Mixte de Recherche*, between the CNRS, EDF and ENSCP. Today, the IRDEP is structured in three activities : (1) R&D aspects of the CISEL project, (2) scale-up of the CISEL process steps, (3) third generation structures and materials. The following contribution limits itself to the presentation of some of our progress in the first of these.

Today at the R&D project level there are two principal short term objectives : (1) small area cells with > 12 % efficiency, and (2) 30 x 30 cm^2 modules with > 8 % efficiency. Our strategy for achieving these goals is to consider alloying Ga and/or S into the $CuInSe_2$, but the present contribution will only discuss the S option. For the S/Se ratio, as is the case for the In/Ga ratio, there are two possible objectives. One is the achievement of "high band gap" materials, i.e. as much S as possible, resulting in high voltage and low current, infrared insensitive devices (less current loss in the window layers), and with lower temperature coefficients, resulting in less discrepancy between true "field" performance and "standard test measurement" performance. The other is to search for the "optimal" band gap relative to small area cells, and "standard test" efficiency measurement procedures. We here recall two composition to bang gap relationships that can found in the literature, both measured from bulk materials [3],[4] :

$$E_g(CuIn_{1-x}Ga_xSe_2) = 1.010 + 0.459x + 0{,}167x^2 \quad \text{(eq.1)}$$
$$E_g(CuInS_{2x}Se_{2(1-x)}) = 1.049 + 0{,}375x + 0{,}130x^2 \quad \text{(eq.2)}$$

2 THE CISEL PROCESS

2.1 The process flow chart

Up until now, the substrate preparation, glass washing and DC-sputtering of the Mo back contact, has been the responsibility of St. Gobain Recherche. These Mo layers are grown on 3 mm thick glass to specifications given by the CISEL project. In the case of electrodeposition, the criterion for the optimization of the Mo layers differs considerable from that of co-evaporated layers. Not only does the Mo play the role of electrode for the electrodeposition itself, but the chemistry and thermal conditions experienced by the Mo are specific to the electrochemical approach.

Upon reception of the Mo coated substrates, the CISEL process flow chart is defined on either 5x5 cm^2 or 30x30 cm^2 substrates. Today, and for both size substrates we master : (1) the electrodeposition of the $CuInSe_2$ precursors, (2) the addition of sulfur to these precursors, (3) a rapid thermal anneal (RTA) resulting in the recrystallization of the precursors, (4) a surface treatment (presently a CN^- etch) required when the films are Cu-rich, (5) "standard" (CBD)CdS buffer layer growth, (6) "standard" RF-sputtered ZnO/ZnO:Al window layer deposition. This flow chart is depicted in Fig. 1.

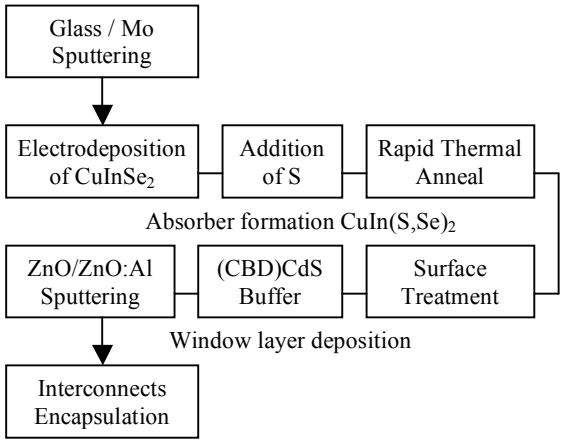

Figure 1: CISEL project process flow chart.

2.2 The electrodeposited precursors

In the present work, one step electrodeposition of $CuInSe_2$ is obtained from acidic aqueous solutions, using sodium or potassium sulfate as supporting electrolyte and containing both SeO_2 and sulfates of Cu and In. By the control of the appropriate ratio of Se/Cu, the appropriate stirring of the bath and the application of a potential between the cathode (where the deposition occurs) and the anode, $CuInSe_2$ can be deposited along with secondary phases of elemental Se and Cu_2Se or In_2Se_3. Detailed studies and literature reviews of this process can be found elsewhere [1], The general reaction for the deposition is :

$$2H_2SeO_3 + Cu^{2+} + In^{3+} + 13e^- + 8H^+ \Leftrightarrow CuInSe_2 + 6H_2O$$

As shown in Fig. 2a and Fig. 2b, we have established deposition conditions where the precursor film morphology is relatively smooth and the film density is relatively high. Usually these films exhibit the presence of some fine crevices (widths of tens of nm) through their upper half and an evolution of the grain size is from 50-100 nm near the back contact to only 10-20 towards the top surface of the films. In Fig. 3 is shown XRD data (measured using a Co source) for a typical slightly Cu-rich precursor. This data shows that this precursor is mostly composed of $CuInSe_2$ and a secondary phase of Cu_2Se, the peak widths are coherent with the small grain sizes seen in the TEM. Cross-sectional EDX measurements of TEM samples reveal that the overall composition is close to uniform in depth, with a slight Cu enrichment towards the back contact and some Cu/In fluctuations from grain to grain. The characteristic scale of these Cu/In fluctuations is the same as that of the average grain size, i.e. 50-100 mn, close to the back contact. and less near the top surface A detailed examination of the rear contact interface show an intermixed zone in the order of 10 nm where Mo, Cu, In and Se seem to be present.

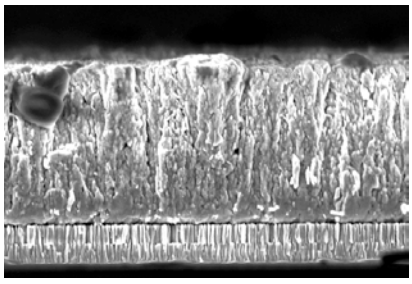

Figure 2a: SEM cross-sectional micrograph of a typical electrodeposited precursor.

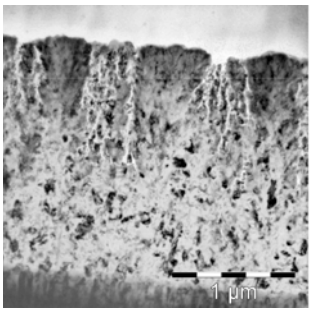

Figure 2b: Bright-field TEM micrograph of a typical electrodeposited precursor. Crevices are observed and average grain sizes can be estimated.

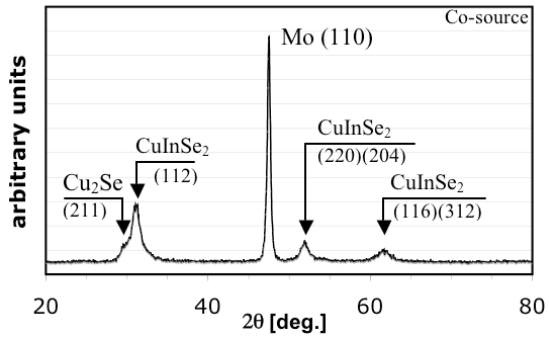

Figure 3: XRD pattern for a slightly Cu-rich precursor.

From a process point of view, both the repeatability and the uniformity of these precursors are examined. When the deposition conditions are fixed (temperature, bath concentrations, applied potential and deposition time), repeatability has been shown by measuring the atomic concentrations of the elements at given positions of our 5x5 cm^2 substrates for over 300 runs. Both the run to run fluctuations and the long term drift of the process are within a few % of the target values. This control chart is shown in Fig. 4, in which the compositions are measured using XFR. Uniformity, on the other hand, is best demonstrated on our 30x30 cm^2 substrates (not shown here) where the relative lateral compositional variations are seen to be < 5%, although thickness variations may be greater (10-20 %). The improvement of the thickness uniformity is in progress (mostly an issue of solution agitation and/or Mo sheet resistance), but the present thickness variations have not been seen to strongly impact the device behavior.

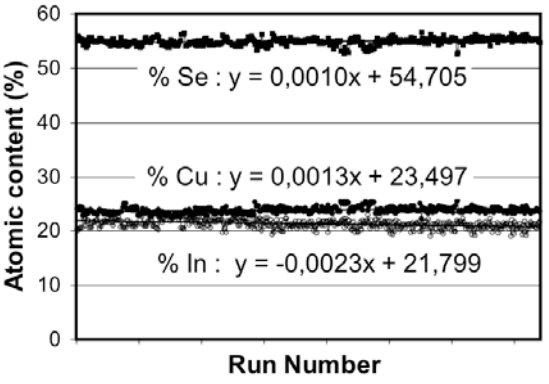

Figure 4: Run to run (XRF measurements) control chart of the electrodeposited precursor composition.

2.3 The addition of S and the recrystallization process

The small grain $CuInSe_2$ precursors can be recrystallized into large grain, device quality material (as will be shown in Fig. 6), but there are a number of reasons (efficiency maximization but also others) to modify this base material towards ones with larger band gaps. For this purpose, the addition of Al, Ga, or S are among common choices. Although the addition of Ga is a research topic at the IRDEP, this present contribution will only discuss that of S. In principal there are four options : (1) co-electrodeposition of sulfur within the precursor, (2) deposition of sulfur or a sulfur containing compound onto the precursor prior to the recrystallization process, (3) recrystallization under a S containing atmosphere, and (4) sulfurization of the recrystallized $CuInSe_2$. The

second of these options is shown in the flow chart in Fig. 1. This process is applied both for our "large gap" objective in which as much S as possible is added so as to result in a material with a band gap as close to that of $CuInS_2$ as possible, and for our "optimal gap" objective in which the idea is to add just enough S so as to result in 1.1 eV < E_g < 1.2 eV. We have shown earlier [2] that the value of x in $CuInS_{2x}Se_{2(1-x)}$ can be adjusted by the quantity of S added to the precursor. This result is recalled in Fig. 5 (remarking that x = S/(S+Se)), but it must be pointed out that this relationship is strongly dependent on the recrystallization (RTA) conditions. According to (eq.2) given in the introduction the "optimal gap" of E_g between 1.1 and 1.2 eV is obtained for values of x between 0.2 and 0.4. For the RTA conditions used in Fig. 5, such a figure can be used as a guideline for the quantity of S needed in the precursor to obtain a targeted E_g values. It is also observable from Fig. 5, that is seems difficult to obtain pure $CuInS_2$, as some 5-10 % Se is persisting in the annealed films, even if high quantities of S are involved in the RTA process.

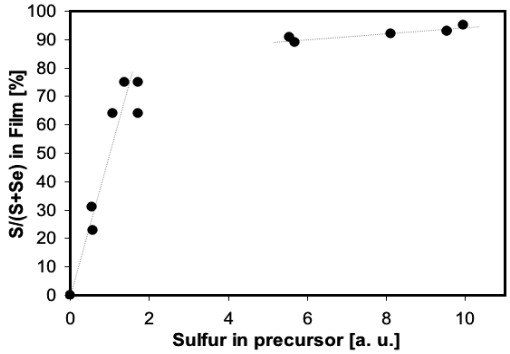

Figure 5: Se to S exchange in the recrystallized film as a function of the S content in the precursor

The recrystallization process that we use is a rapid thermal anneal under an argon atmosphere. Our equipment permits us to handle substrates up to 30x30 cm^2, but these are often cut down to smaller sizes in order to increase our experimental possibilities. One commonly used size is 11x11 cm^2 (one quarter of a 30x30 cm^2, minus the "edges"), but we also work on smaller substrates of 1x2.5 cm^2 and 2.5x2.5 cm^2. It is clear that relative to substrate breakage issues, the larger substrates impose more restrictive thermal conditions.

In Fig. 6 are shown cross-sectional SEM micrographs of finished devices using CISS layers grown for different sulfur contents. The values of the S/(S+Se) ratios for these films being : 90-95 %, ≈ 40 % and 0 %. For the chosen micrographs it is seen that the lower the sulfur content, the larger the grain size. It must be remarked that from a statistical point of view this trend may be even stronger than that seen in Fig. 6. For the high S-content case, we have often found that the obtained grain sizes can be even smaller than the ones show in Fig. 6, many other factors having their impact on this issue. On the other hand, the grain sizes in the low-S, or no-S case are much more commonly as show in Fig. 6, the impact of the "other factors" being less sensitive when less sulfur is involved. From this Fig. 6 it can also be seen that our recrystallized film thickness is between 1.5 and 2 μm, which is in the same order as the thickness of the precursors from which these films are produced.

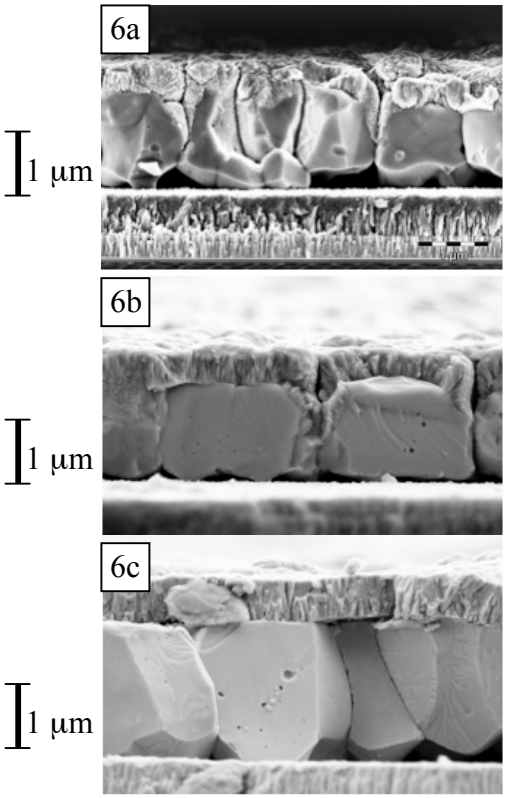

Figure 6: SEM cross-sections of finished devices for different sulfur contents.
6a: S/(S+Se) ≈ 95 % (wide gap)
6b: S/(S+Se) ≈ 40 % ("optimal" gap)
6c: S/(S+Se) = 0 % (i.e. without sulfur)

2.4 The surface treatment

The CISS films shown in Fig. 6 were all obtained from Cu-rich precursors as those shown in Fig. 2 and Fig. 3. The Cu/In ratios, measured by X-ray florescence, of these precursors were between 1.1 and 1.2, but these ratios increased to between 1.2 and 1.4 by the RTA process. This indicates an In-loss mechanism during the RTA process, despite the fact that the precursors were Cu-rich and were believed to be composed (at least from an XRD point of view) of phases of $CuInSe_2$ and Cu_2Se. The result is that the recrystallized films require the application of an etching step, we here apply the commonly used CN^- etch, known to remove Cu_2Se or CuS without substantial attack of either the $CuInSe_2$ or the $CuInS_2$ phases. Our XRF data shown post etched layers to be consistently very close to stoechiometry (Cu/In ≈1, with some offset from unity that may be due to measurement calibration).

In Fig. 7 is shown a comparison of the XRD patterns (measured using a Co source) of a precursor (identical to Fig. 3), of a sulfurized and recrystallized layer, and of this same layer after the CN^- etch. In these XRD patterns we can see that the poorly resolved (112), (204)(220), and (116)(312) peaks of the small grain $CuInSe_2$ precursor are shifted towards higher angles indicating an almost complete substitution of the Se by S, in good accordance with the S/(S+Se) ratios measured by XRF. Also, the resolution and amplitude of these peaks are increased (improved crystallinity), and many other minor $CuInS_2$ peaks become observed. As can be expected by the fact that this recrystallized layer is Cu-rich and

annealed under excess S, a number of peaks ((102), (103), (006), (110) and (108)) from the CuS phase are also observed. These peaks are "cleanly" removed (i.e. without influencing the rest of the $CuInS_2$ signature) by our CN^- etching step as can be seen in Fig. 7. We also remark that there appears to be a small shift towards lower angles of the Mo (110) peak position by the RTA process, this observation remains to be confirmed and studied, but may be a real effect of the RTA on the Mo back contact layer.

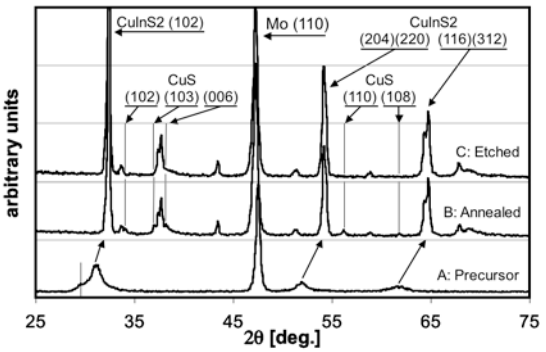

Figure 7: Evolution of the XRD patterns through the various steps of the CISS layer processing.
A: Electrodeposited precursor (Cu-rich)
B: After the RTA-recrystallization
C: After the CN^- surface treatment

2.5 NH_3-free (CBD)CdS buffer layer process

For our "standard" devices we use the "standard" CBD process for CdS deposition, consisting in an NH_3 based solution containing Cd^{2+} ions and thiourea at a pH of 10.5 and a deposition temperature of 60 °C. Motivated by the idea of avoiding the use of NH_3 and replacing it by a less volatile substance, a bath chemistry based on sodium citrate has been developed [5]. This NH_3-free formulation results in bath conditions where the pH is equal to 12.0 and the deposition can occur keeping the "standard" bath temperature of 60 °C, but as this growth is slower, we have also used higher bath temperatures (70 °C) so as to result is more similar growth kinetics to the standard conditions. We also compare these CdS growths to ones using NH_3 but in which the pH is adjusted up to 12.0 by the addition of NaOH. By using slightly different total deposition times we have grown (CBD)CdS layers on either glass substrates or CISS substrates which appear to result in equal thicknesses and equal coverage quality from all of these bath formulations. The optical transmissions of these layers on glass are shown in Fig. 8, where the different growth times are indicated.

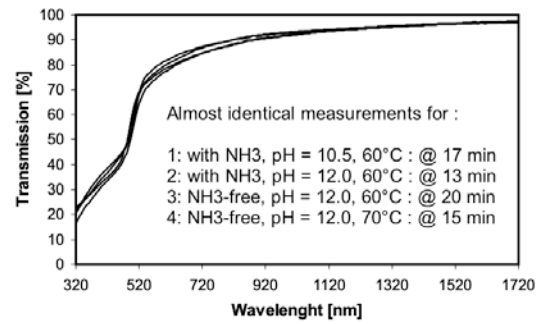

Figure 8: Optical transmissions of the (CBD)CdS films on glass from the different bath formulations.

For the chosen deposition times, almost identical T(λ) measurements show that the (CBD)CdS films are almost identical from their optical and thickness point of view. Nevertheless, these different bath formulations have resulted in remarkably different device qualities, our NH_3 containing standard (pH=10.5) being the best, but followed closely by the NH_3 containing, readjusted to pH=12.0 conditions. On the other hand the NH_3-free formulations have led to very poor Voc and FF values. In the present case, a particularly interesting point is that all the absorbers had been CN^- etched prior to the (CDB)CdS deposition. This seems to indicate that, even immediately after a CN^- etch, the role of the NH_3 on the CISS surface seems to be critical. These questions are under further investigation.

2.6 Back Contact Issues

In our process the back contact Mo layer is often considerably sulfurized and selenized. This results in a thick $Mo(S,Se)_2$ layer, consuming a variable fraction of the Mo back contact. In Fig. 9 is shown a SEM micrograph of the back contact layer after the RTA process. The difference between the pure Mo fraction and the $Mo(S,Se)_2$ fraction of the back contact is clearly visible, the interface between the two being apparently abrupt and planar. As can be expected, the thickness of this $Mo(S,Se)_2$ is controlled by the time-temperature profile of the RTA process, but not uniquely, other controlling parameters being equally important. As expected from the large volume increase which occurs as Mo is converted to $Mo(S,Se)_2$, the total thickness of the Mo + $Mo(S,Se)_2$ is considerably more than the original Mo layer thickness.

HR-TEM studies of thin samples prepared from similar layers to that of Fig. 9 show the $Mo(S,Se)_2$ to be oriented with the (002) planes perpendicular to the substrate (images not shown here). This orientation, sometimes referred to as type 1, is that which is acceptable from an adhesion point of view of the CISS on the back contact. On these TEM samples we have measured the inter-reticular distance (distance between two adjacent Mo planes) to be 6.97 Å. Values commonly reported in the literature for single crystals of pure MoS_2 are close to 6.15 Å [6]. EDX measurements across the TEM sample are shown in Fig. 10. It is clearly shown that : (1) the Mo/$Mo(S,Se)_2$ interface is abrupt, (2) there is little Se, (3) there is a considerable amount of Cu in these films. This Cu is probably intercalated between the Van der Waals planes of the MoS_2 or $Mo(S,Se)_2$ and may, at least partially, explain the larger measured value of the inter-reticular distance. No In is found in this layer.

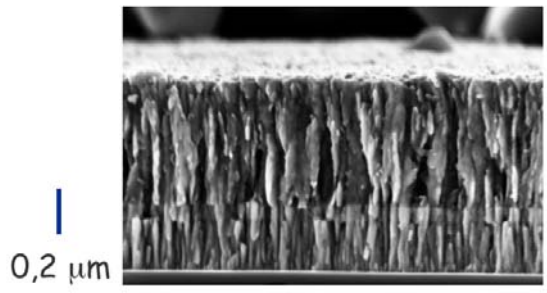

Figure 9: Cross-sectional SEM micrograph of the back contact after the RTA-recrystallization of the CISS film. A two layer structure is clearly visible.

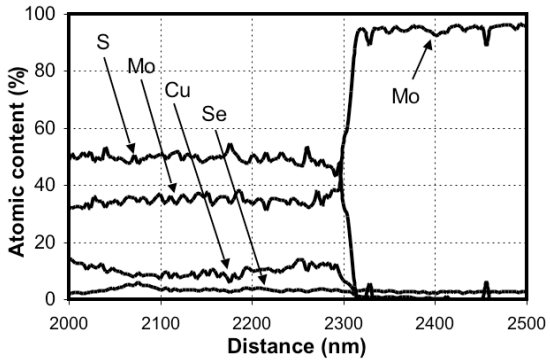

Figure 10: EDX measurements across the back contact layer, showing the compositions of the two zones.

2.7 Cell Results

Since the last European conference in Paris, we have improved our record device efficiency to 11.5 % with Voc = 722 mV, Jsc = 23.8 mA/cm^2 and FF = 67 %. This device is measured without the use of a grid (and thus from a small active area of 0.1 cm^2) and without the use of an anti-flexion coating. The quantum efficiency of this device exhibits a band gap cut-off at 1.47 eV in accordance with the very high sulfur content (S/(S+Se)) in the order of 95 %. What we have progressed on considerably is the improvement of the control of device quality and reproducibility, as measured by the statistical spread, both across a substrate of multiple devices, as well as from run to run. Today the standard deviation of our standard devices is approximately ± 1 %. An example of this is shown in Fig. 12 for a substrate, shown in Fig. 11, resulting from a 30x30 cm^2 precursor, that had been cut down to 11x11 cm^2 pieces prior the RTA-recrystallization step. The devices across this substrate, using the grid design from the Angstrom Solar Center (ASC), may not be of the highest efficiency, but show excellent uniformity on this 11x11 cm^2 sample, as well as between the other three 11x11 cm^2 samples from the same 30x30 cm^2 precursor. From this result, we are confident that the quality of the 30x30 cm^2 precursor is uniform, at least at this 7 % level when associated to the present state of the other process steps.

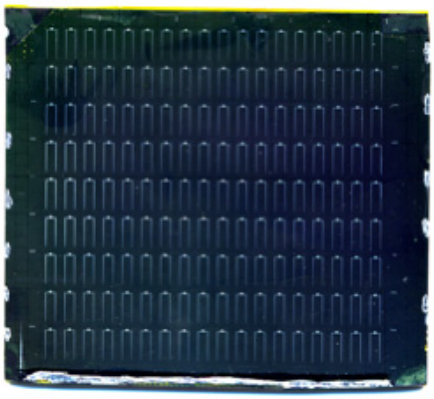

Figure 11: Array of gridded devices on an 11x11 cm^2 sample. Four such samples are cut-down from a 30x30 cm^2 precursor and RTA processed separately. This sample has 9 rows of 18 cells (i.e. 162 devices). Each cell has an area of 0.5 cm^2 using the grid design from the ASC.

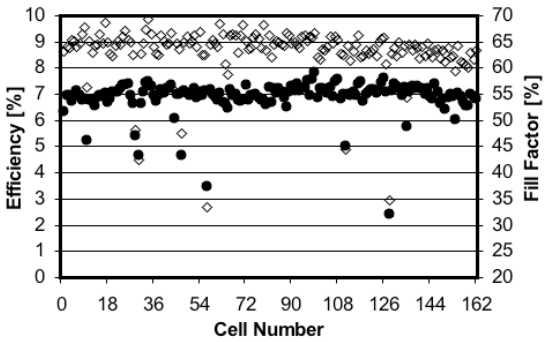

Figure 12: Efficiency (solid circles) and fill factor (open squares) uniformity across the 162 devices of sample shown in Fig. 11.

3 CONCLUSIONS

Progress in the CISEL project is shown. Some detailed structural and compositional material characterization (SEM, TEM, XRD, XRF) of the layers is performed, in particular in regard to the recrystallization of the precursors. Grain size to sulfur content trends are confirmed. The impact of the RTA-recrystallization process on the Mo back contact is shown to result in a thick $Mo(S,Se)_2$ oriented with the (002) planes perpendicular to the substrate and containing a considerable amount of Cu. An alternative NH_3-free (CBD)CdS process is shown to successfully grow CdS but does not result in quality devices. Uniformity of cell results from 30x30 cm^2 precursors is shown.

ACKNOWLEDGMENTS

The authors thank the ADEME for its financial support and all the participants of the CISEL project for the elaboration of the films and of the devices.

REFERENCES

[1] D. Lincot, J.F. Guillemoles, S. Taunier, D. Guimard, J. Sicx-Kurdi, A. Chomont, O. Roussel, O. Ramdani, C. Hubert, J.P. Fauvarque, N. Bodereau, L. Parissi, P. Panheleux, P. Fanouillère, N. Naghavi, P.P. Grand, M. Benfarah, P. Mogensen, O. Kerrec, *Solar Energy*, **77** (2004) 725

[2] S. Taunier, J. Sicx-Kurdi, P.P. Grand, A. Chomont, O. Ramdani, L. Parissi, P. Panheleux, N. Naghavi, C. Hubert, M. Ben-Farah, J.F. Guillemoles, D. Lincot, P. Mogensen, O. Kerrec *et al. Thin Solid Films,* **480-481** (2005) 526.

[3] M. Alonso, M. Garriga, C. Durante Rincón, E. Hernández, M. León, *Appli. Phys.* A **74** (2002) 659

[4] A.V. Mudryi, I.A. Victorov, V.F. Gremenok, A.I. Patuk, I.A. Shakin, M.V. Yakushev, *Thin Solid Films* **431-432** (2003) 197

[5] N. Naghavi, C. Hubert, O. Roussel, L. Sapin, M. Lamirand, J.-F. Guillemoles, D. Lincot, J. Kessler O. Kerrec, *to be published*, presented at the MRS Spring meeting 2005, San Francisco

[6] F. Jellinek, G. Brauer, H. Muller, *Nature* **185** (1960) 376